Controlling the Morphologies of Organometallic Block Copolymers in the 3-Dimensional Spatial Confinement of Colloidal and Inverse Colloidal Crystals

David A. Rider,[†] Jennifer I. L. Chen,[†] Jean-Charles Eloi,[‡] André C. Arsenault,[†] Thomas P. Russell,[§] Geoffrey A. Ozin,*[,†] and Ian Manners*[,‡]

Department of Chemistry, University of Toronto, Toronto, ON, M5S 3H6, Canada, School of Chemistry, University of Bristol, Bristol, BS8 1TS, U.K., and Polymer Science and Engineering Department, University of Massachusetts, Amherst, Massachusetts 01003

Received September 7, 2007; Revised Manuscript Received December 19, 2007

ABSTRACT: A detailed study of the three-dimensional (3-D) confinement of polystyrene-*block*-poly(ferrocenylethylmethylsilane) (**PS-*b*-PFS**) diblock copolymers in silica colloidal crystals and inverse silica colloidal crystals is reported. Inversion of the silica colloidal crystal lattice with **PS-*b*-PFS** is confirmed by scanning electron microscopy and optical spectroscopy. Additionally, the modification of the silica surfaces in the inverse colloidal crystals using hydroxy-terminated **PS** and **PFS** is established. The 3-D confined morphologies of a lamella-forming and a cylinder-forming **PS-*b*-PFS** diblock copolymer are subsequently investigated. The manipulation of the 3-D confined morphology of cylinder-forming **PS-*b*-PFS** is demonstrated by deliberate alteration of its wetting interaction with the surface-modified colloidal crystal templates. Unprecedented 3-dimensional block copolymer morphology transitions are elucidated.

Introduction

The bulk equilibrium morphologies of diblock copolymers have been extensively studied experimentally and theoretically.[1] It is well-known that the volume fraction of one block dictates the resulting morphologies which are typically ordered spheres, cylinders and lamellae. Confinement is a powerful tool in breaking the symmetry of a structure, thus allowing materials to demonstrate new behavior.[2−12] To this end, the one- and two-dimensional (1-D and 2-D) confinement of diblock copolymers has led to morphological transitions.[8,13] Relatively unexplored to date in this respect is the three-dimensional (3-D) confinement of diblock copolymers. A further means for morphology manipulation is available through mediation of interfacial interactions.[14−18] In the bulk, diblock copolymers microphase separate into arrays of domains with a characteristic equilibrium period, L_0.[19] In thin films, interactions between the domains and the air and substrate interface can cause segregation of one of the blocks to these interfaces (wetting).[20−31] For lamella-forming diblock copolymers, if the same block is present at both interfaces (symmetric wetting) then the film thickness is defined by nL_0, where n is an integer. The film thickness in the case of asymmetric wetting is therefore defined by $(n + 0.5)L_0$. When n is nonintegral, the lattice is incommensurate in the film thickness and typically leads to islands or holes (defined by heights of step length L_0) at the air−film boundary. For thin films between two solid and planar interfaces with 1-D interspacing distance D_1, this varied topography is not permitted. The frustration of incommensurability is therefore strongest for low D_1/L_0 ratios. With significant 1-D commensurability frustration, the lamellar lattice is forced to respond either through changes in L_0 or through elimination of wetting interactions. It follows, therefore, that for 2- and 3-D analogues, the respective comensurability frustration criteria are also described by their D_2/L_0 and D_3/L_0 ratios, respectively.

We recently described the confinement of lamella-forming diblock copolymers using a 3-D colloidal crystal (CC) template approach.[32] We utilized the excellent electron density contrast and elemental mapping made possible by the use of iron-rich polyferrocenylsilane (**PFS**) block to define the nature of the microphase separation in 3-D confinement.[33] Further interest arises as these materials are magnetic ceramic and catalyst precursors,[34−37] and exhibit reversible redox-tunable properties.[38−41] A lamella-forming and a cylinder-forming polystyrene-*block*-poly(ferrocenylethylmethylsilane) (**PS-*b*-PFS**) diblock copolymer are used in this study. We present herein a thorough investigation on the self-assembly of three-dimensionally confined **PS-*b*-PFS** in a series of colloidal crystal templates. Moreover, we demonstrate the manipulation of the 3-D confined morphology of cylinder-forming **PS-*b*-PFS** through deliberate alteration of its wetting interaction of its template. By these means, unprecedented 3-dimensional block copolymer morphology transitions are reported.

Results and Discussion

The **PS-*b*-PFS** diblock copolymers used in this study are described in Table 1. The polydispersity indices, as determined by gel permeation chromatography equipped with a triple detector, were below 1.10 in all cases. Throughout this article each will be described according to the following nomenclature, **PS-*b*-PFS** (ϕ_{PFS}), where the bracketed fraction denotes the volume ratio of **PFS** (ϕ_{PFS}). To control the surface interactions between the colloidal crystal (CC) lattices and the block copolymer confined within, hydroxy-terminated **PS** (**PS—OH**) and hydroxy-terminated **PFS** (**PFS—OH**) were used. The molecular characteristics of the homopolymers and diblock copolymers are summarized in Table 1.

Bulk Morphologies of PS-*b*-PFS Block Copolymers. The equilibrium bulk morphologies of the **PS-*b*-PFS** diblock co-

* Corresponding author. E-mail: (G.O.) gozin@chem.utoronto.ca; (I.M.) ian.manners@bristol.ac.uk.
[†] Department of Chemistry, University of Toronto.
[‡] School of Chemistry, University of Bristol.
[§] Polymer Science and Engineering Department, University of Massachusetts, Amherst.

10.1021/ma7020248 CCC: $40.75
Published on Web 03/04/2008

Table 1. Characteristics of the Homopolymers and Diblock Copolymers Used in This Study

polymer	M_n(PDI)[a]	ϕ_{PFS}	bulk morphology	L_0 (nm)
PS—OH	9900 (1.05)	0		
PFS—OH	8100 (1.17)	~1.00		
PS-*b*-PFS (0.36)	68 200 (1.04)	0.36	hex. PFS cylinders	43[b]
PS-*b*-PFS (0.52)	132 000 (1.05)	0.52	lamellar	88[c]

[a] From GPC curve. Standard deviation for M_n and PDI estimated to be ~5% and ~1%, respectively. [b] Bulk $L_0 = 4\pi/(\sqrt{3} \times q^*)$; where q^* is the primary scattering peak as determined by small-angle X-ray scattering. Bulk $d_{cyl} = 2\sqrt{(D_{c-c}^2 \times \phi_{PFS}/\pi)}$; where the volume prism defined by three cylinders contains half a cylinder in its volume. [c] Estimated from high-resolution TEM images.[42,43]

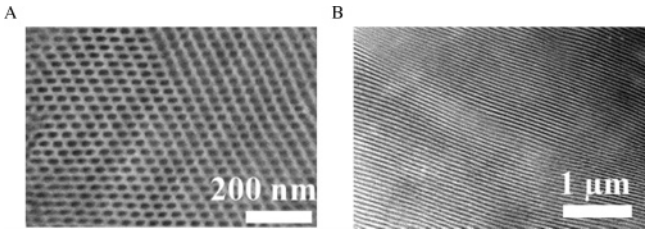

Figure 1. Representative BF-TEM images of **PS-*b*-PFS** materials used in this study. (A) **PS-*b*-PFS (0.36)**. (B) **PS-*b*-PFS (0.52)**.

polymers were produced by slow casting from toluene or benzene for 1 week, drying overnight at 50 °C, and thermally annealing at 170−190 °C for 48−96 h.[42] Bulk samples were mounted on a cured acrylate-based resin with a cyanoacrylate glue and subsequently sectioned for transmission electron microscopy (TEM). All samples were imaged without staining, as the high electron density associated with the main chain Fe atoms provided sufficient contrast for TEM micrographs. For bright field TEM (BF-TEM) images, **PFS** areas are dark whereas **PS** areas are lighter. For dark field TEM (DF-TEM), the contrast is inverted and thus **PFS** areas are lighter whereas **PS** areas are dark. The bright field TEM images and depictions of the bulk morphologies of the **PS-*b*-PFS** block copolymers used throughout this study are shown in Figure 1. For lamella-forming **PS-*b*-PFS,** the average **PFS** and **PS** lamella thickness of 46 and 42 nm, respectively, and average domain spacing of 88 nm were determined by BF-TEM. For cylinder-forming **PS-*b*-PFS**, the **PFS** cylindrical diameter (d_{cyl}) and equilibrium periodicity (L_0) are ~29 nm and ~43 nm and were determined by small-angle X-ray scattering, respectively.

Preparation and Infiltration of Colloidal Crystal Templates. Scheme 1 illustrates the 3-D confinement approach we have used. For nomenclature purposes, the colloidal crystals (CC) will be referred to as described in the schematic. When further detail is required, a subscript will be used to describe the composition of the spheres in the lattice. The CC templates, CC $\mathbf{1}_{\mathbf{silica}}$ and CC $\mathbf{1}_{\mathbf{PS}}$, are obtained from the self-assembly of silica and polystyrene microspheres, respectively. Inversion of CC $\mathbf{1}_{\mathbf{PS}}$ with silica affords CC $\mathbf{4}_{\mathbf{air}}$.[9] Only silica or brushed-silica CC templates are used throughout this study and thus CC $\mathbf{1}_{\mathbf{silica}}$ and CC $\mathbf{4}_{\mathbf{air}}$ are the parent CCs for our 3-D confinement approach. Transmission UV−visible (UV−vis) spectroscopy was used for optical characterization of the experimental Bragg diffraction peak and this was compared with the theoretical estimate as determined by a scalar-wave approximation.[44] This approach has been shown to be very effective at characterizing the thickness and volume composition of CCs.[45]

To effectively study the 3-D confinement of diblock copolymers, the complete infiltration of CC scaffolds is critical. For infiltration, dichloromethane solutions of **PS—OH**, **PFS—OH**, or **PS-*b*-PFS** were allowed to evaporate in the presence of a template from Scheme 1. Following evaporation and thermal annealing, the silica templates were removed using $HF_{(aq)}$ (***CAUTION!***) to reveal a polymer lattice which was subsequently investigated by scanning electron microscopy (SEM). Representative SEM images of 3-D confined **PS-*b*-PFS** as CC **3** and CC **6** (**PS-*b*-PFS (0.52)** and **PS-*b*-PFS (0.36)**, respectively) are shown in Figure 2, parts A and B, respectively. Similar SEM images were found for all polymer-infiltrated and HF-etched CCs. As suggested by the uniformity of the microstructure found in these images, the above procedure is effective for replacing voids in the CC templates quantitatively with **PS—OH**, **PFS—OH**, or **PS-*b*-PFS**.

Since CC **6**, and its precursors CC **4** and **5**, consisted of a lattice of 220 nm diameter spheres, monitoring the changes of the Bragg diffraction characteristics in the UV−visible region is possible. In this case, CC **4** was found to have a Bragg diffraction peak at $\lambda_{max} = 408$ nm, a value which agrees with its theoretical estimate (see Figure 3A or Table 2, entry A). Upon complete infiltration, it is anticipated that, due to the replacement of the air voids (refractive index, n, =1.0) with **PS-*b*-PFS**, **PS—OH**, or **PFS—OH** (for simplicity all assumed to have $n \sim 1.6$), a shift in the Bragg peak to $\lambda_{max} = 574$ nm would occur. Experimentally, CC **5**, CC **7** and CC **11** exhibited Bragg λ_{max} values of 572, 564, and 578 nm, respectively (see Figure 3B or Table 2, entries B, D, and H).

To study of the effects of preferential surface interactions with the CC templates for 3-D confined block copolymers, we prepared two additional CCs. The **PS**- and **PFS**-brushed templates, CC $\mathbf{8}_{\mathbf{PS\ brush/air}}$ and CC $\mathbf{12}_{\mathbf{PFS\ brush/air}}$, were prepared through a condensation reaction of surface hydroxyl groups of the silica CC with that of the hydroxy-terminus of **PS—OH** and **PFS—OH** in CC **7** and CC **11**, respectively. For the representative CC **8**, infiltration with a dichloromethane solution of **PS—OH** produced structure CC **7** which was subsequently heated for 3 days at 170 °C. During this procedure, the **PS** homopolymer was successfully grafted to the silica surface. Repeated rinsing with toluene removed excess **PS—OH** to afford CC **8**. The new Bragg diffraction peak for **8** at $\lambda_{max} =$ 431 nm (Table 2, entry E) was used to determine a brush layer thickness of 7 nm (~ 17 vol % of original sphere void), a value that agrees with literature on homopolymer and random copolymer grafting onto planar surfaces.[16] For the CC **12**, the λ_{max} shifted to 422 nm (Table 2, entry I) with ~ 13 vol % of the original sphere being occupied by the **PFS** layer. This corresponds to a **PFS** brush layer thickness of 5 nm. As two additional control experiments, CC **4** was (i) treated to the identical thermal treatment as above and (ii) filled with **PS—OH** to produce CC **7** and, without heating for 3 days, emptied via the toluene extraction procedure. In both cases, it was found that the Bragg characteristics were within experimental error of that for CC **4** (see Table 2, entries J and K respectively). Attempted isolation of the **PS** from the $HF_{(aq)}$ etched CC $\mathbf{8}_{\mathbf{PS\ brush/air}}$ was not possible due to the extreme fragility of the lattice, which is supposedly destroyed in the $HF_{(aq)}$ etching and drying steps. Molecular weight characterization of the brush layers was attempted using GPC on extracts of the residue from the dried $HF_{(aq)}$ etchant as well as by direct MALDI−TOF spectroscopy on CC $\mathbf{8}_{\mathbf{PS\ brush/air}}$ and CC $\mathbf{12}_{\mathbf{PFS\ brush/air}}$ using 1,8,9-anthracentriol as a charge matrix. In all cases, no molecular weight signal was detected likely due to the extremely small amount of **PS** and **PFS** in the CCs (for a typical 1 cm^2 sample area and a **PS** or **PFS** layer thickness of 7 nm, $\sim 10^{-2}$ mg) and their strong covalent adhesion to the support silica.

Scheme 1. Preparation of Colloidal Crystal Templates (CC 1, 4, 8, and 12) and 3-D Confined PS-*b*-PFS Colloidal Crystals (CC 2, 3, 5, 6, 9, 10, 13, and 14)[a]

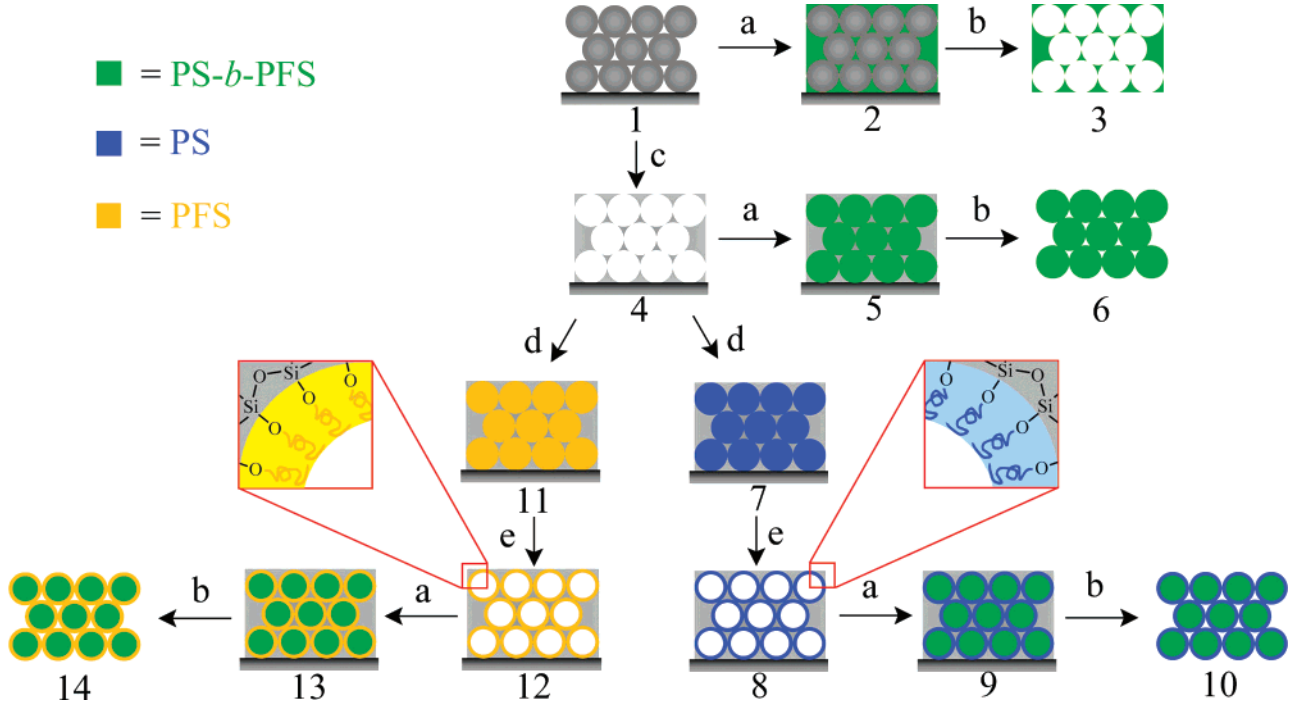

[a] Key: (a) Capillary infiltration with **PS-*b*-PFS**. (b) Annealing and removal of silica template by aqueous HF (***Caution!***). (c) CC $\mathbf{1}_{PS}$, inversion via silica CVD. (d) Capillary infiltration with **PS—OH** or **PFS—OH** for CC **7** and **11**, respectively. (e) Grafting **PS** or **PFS** (for CC **8** and **12**, respectively) to silica via treatment at 170 °C/3 days and then rinsing with excess toluene.

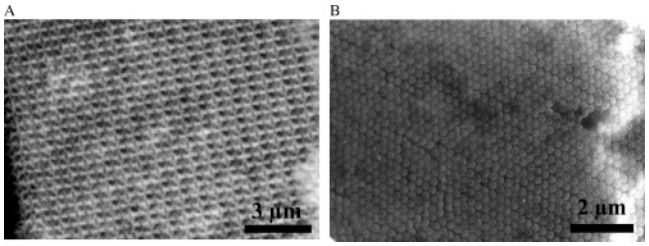

Figure 2. Representative SEM images of (a) CC **3** (**PS-*b*-PFS (0.52)**; sphere size = 850 nm) and (b) CC **6** (**PS-*b*-PFS (0.36)**; sphere size = 220 nm).

Morphology of 3-D Confined Lamellar-Forming PS-*b*-PFS Block Copolymers as CC 3. Solution infiltration and annealing of the lamellar-forming diblock copolymer **PS-*b*-PFS (0.52)** in CC $\mathbf{1}_{silica}$ having silica sphere diameters from 375 to 850 nm led to novel microphase-separated morphologies which are highly unusual. Because of the strong confinement imposed by the surrounding silica spheres ($D_3/L_0 = 1.8$ and 0.9 for 375 nm CC **1** octahedral and tetrahedral holes; $D_3/L_0 = 4.1$ and 2.0 for 850 nm CC **1** octahedral and tetrahedral holes, respectively), the lamellae orient themselves orthogonal to the sphere surfaces instead of in a parallel arrangement most common in lamellar phases.[23] This effect is reminiscent of 1-D confined symmetric diblock copolymers.[30] The periodic and interconnected nature of the silica template forces the lamellae to curve, branch and join, forming a phase that follows the topology of the void space (see Figure 4). Therefore, for the tetrahedral and octahedral sites in the colloidal crystal, tetrapodal and octapodal **PS** domains exist at the center of these sites. The domain assignment was confirmed by energy-dispersive X-ray (EDX) mapping, with C, Fe and Si distribution maps (Figure 4C) showing the location of the **PFS** segments. For the cases with diameters of 375 and 850 nm, 5 and 13 individual unbranched, curved lamellae are typically found between podal domains, where the TEM-estimated periodicity of these **PFS** and **PS** domains ($L_0 \sim 51-72$ nm) is lower than that of its bulk morphology ($L_0 = 88$ nm).

Morphology of 3-D Confined Lamellar-Forming PS-*b*-PFS Block Copolymers as CC 6. Solution infiltration and annealing of the lamellar-forming **PS-*b*-PFS** in CC $\mathbf{4}_{air}$ having air sphere diameters of ~ 210 nm led to a novel core-multishell microphase-separated morphology. Shown in Figure 5A is a DF-TEM showing **PS-*b*-PFS** regions of ca. 210 nm in diameter surrounded by air voids. In this sample, the lamellae were clearly oriented parallel to the templating silica surfaces. While this is the conventional form of lamellar alignment, the strong curvature of the template results in the lamellae wrapping together to form concentric shells with a solid spherical center. This morphology has also theoretically been predicted for 3-D confined symmetric diblock copolymers.[5] Figure 5B shows a DF-TEM image with superimposed EDX elemental traces, confirming the location of the **PS** and **PFS** blocks and the absence of the silica template (see O trace at baseline in Figure 5B). The estimated dimensions by TEM of the **PFS** core and subsequent shell are 98 and 38 nm, respectively, while the inner and outer **PS** shells are 25 and 14 nm, respectively. Clearly the effects of strong 3-D confinement ($D_3/L_0 = 2.4$) have altered both the morphology and dimensions of the lamellar diblock copolymer in comparison to its equilibrium bulk state. In addition to the strong curvature of the void spaces, the surface wetting of the silica template, by **PS** segments in this case, influences the resulting morphology.[46]

Morphology of 3-D Confined Cylinder-Forming PS-*b*-PFS Block Copolymers as CC 6. Considerably more complex is the 3-D confinement of asymmetric cylinder-forming **PS-*b*-PFS** block copolymers. Following our procedures for confinement, the **PS-*b*-PFS (0.36)** was confined in CC **4** to produce the CC **6**. By direct DF-TEM (Figure 6A), a novel and complex morphology was found whose exact structure remains difficult to assign. We have also extensively investigated the surface

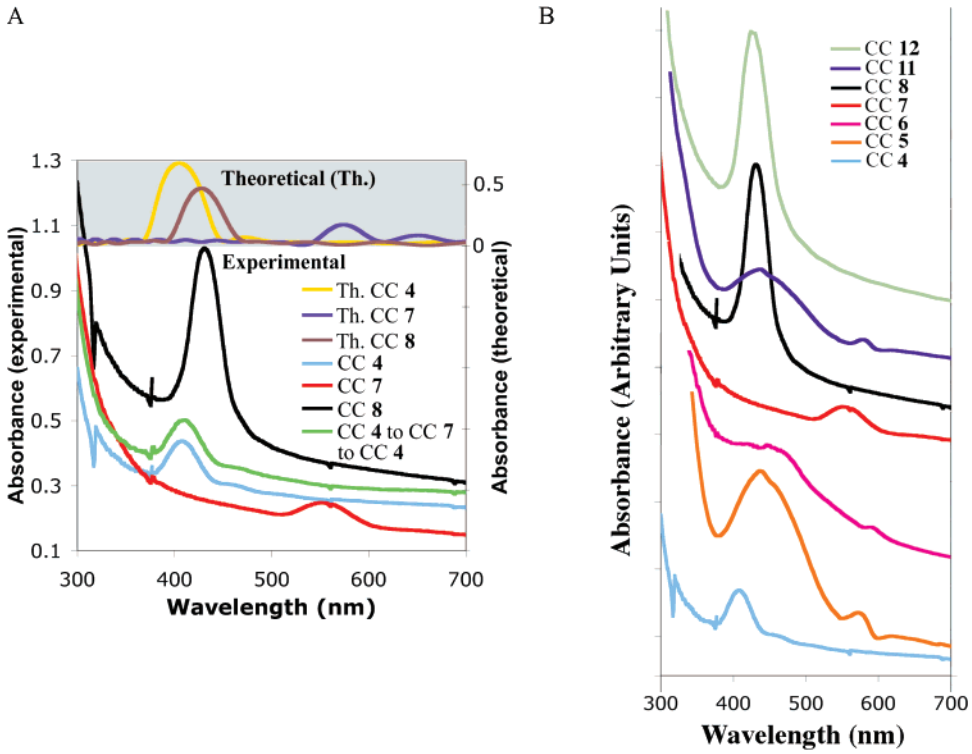

Figure 3. (A) Experimental and theoretical UV−vis spectra characterizing grafting of **PS—OH** to CC **4**. (B) UV−vis spectra characterizing selected **PS-*b*-PFS (0.36)** colloidal crystals used in this study. For CC **5**, CC **6**, and CC **11**, a broad absorption at ∼ 440 nm is present due to large amounts of **PFS** material in the CCs. Spectra were vertically offset for clarity.

Table 2. Comparison of Theoretical and Experimental Bragg Diffraction for Selected PS-*b*-PFS (0.36) Colloidal Crystals (Sphere Size = 220 nm) from Scheme 1

entry	colloidal crystal	theoretical Bragg λ_{max} (nm)[a,b]	experimental Bragg λ_{max} (nm)
A	**4**	404	408
B	**5**	574	572
C	**6**	578	584
D	**7**	574	564
E	**8**	431[e]	431
F	**9**	574	581
G	**10**	578	
H	**11**	574	578
I	**12**	422[f]	422
J	$\mathbf{4}_{170\ °C/3d}$[c]	404	400
K	**4** → **7** → **4**[d]	404	405

[a] On the basis of a scalar-wave approximation for 220 nm sphere size. [b] Assuming $n_{PS} \sim n_{PS-b-PFS} \sim 1.60$; $n_{silica} \sim 1.43$ and $n_{air} = 1$. [c] Control experiment where CC **4** is heated at 170 °C for 3 d. [d] Control experiment where CC **4** is infiltrated with **PS—OH** and subsequently voided via repeated rinsing with toluene. [e] On the basis of 17 vol % of the original sphere volume being occupied by the **PS** brush. [f] On the basis of 13 vol % of the original sphere volume being occupied by the **PFS** brush.

of this sample by scanning force microscopy (SFM) (see Figure 6B) and detected a semi-ordered dotted surface suggesting that both **PS** and **PFS** are present at the outermost surface of the structure. For more accurate investigations of the internal structure, microtoming the sample at thicknesses ∼150 nm revealed further detail. As shown in the DF-TEM image in Figure 6C, random patterns of meandering "cylindrical-like" domains of **PFS** were found in all cases and suggested that the cylinder-forming character of the block copolymer was still present. We conclude therefore that a disordered cylindrical morphology is housed within the semi-ordered structure as observed by SFM. At the surface therefore, a plausible interpretation of the morphology is depicted in Figure 6A and is reminiscent of a "golf-ball" type morphology of the **PFS** domains.[47]

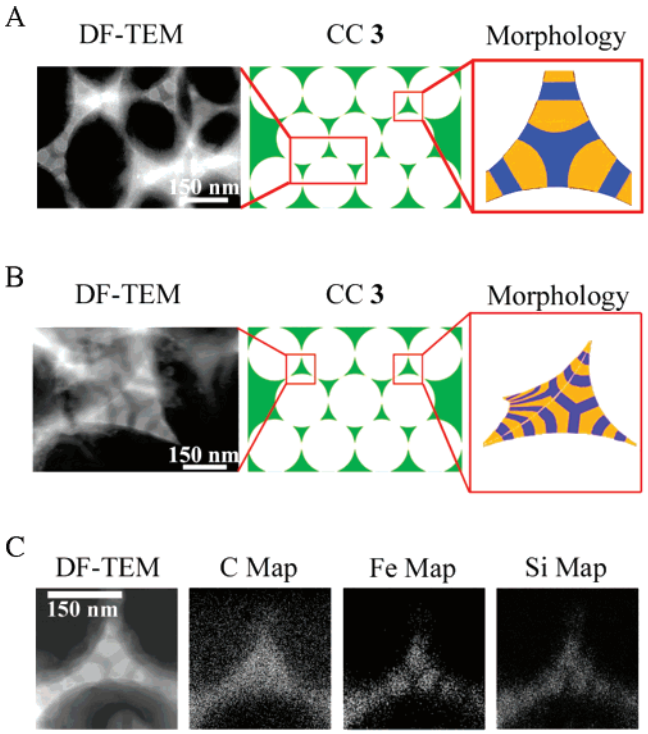

Figure 4. DF-TEM images and depictions of 3-D confined lamella-forming **PS-*b*-PFS (0.52)** in (A) CC_{silica} **1** (sphere diameter = 375 nm) and (B) CC_{silica} **1** (sphere diameter = 850 nm). (C) TEM-EDX mapping of **PS-*b*-PFS (0.52)** in CC_{silica} **1** (sphere diameter = 375 nm) with imaged area, C, Fe and Si maps depicted left to right, respectively.

Controlled Wetting of Templates via a PS Brush Layer and Resulting Morphology of 3-D Confined Cylinder-Forming PS-*b*-PFS Block Copolymers as CC 10. To manipulate the complex morphology arising from the 3-D confinement of cylinder-forming **PS-*b*-PFS** in CC **6**, we explored the use of

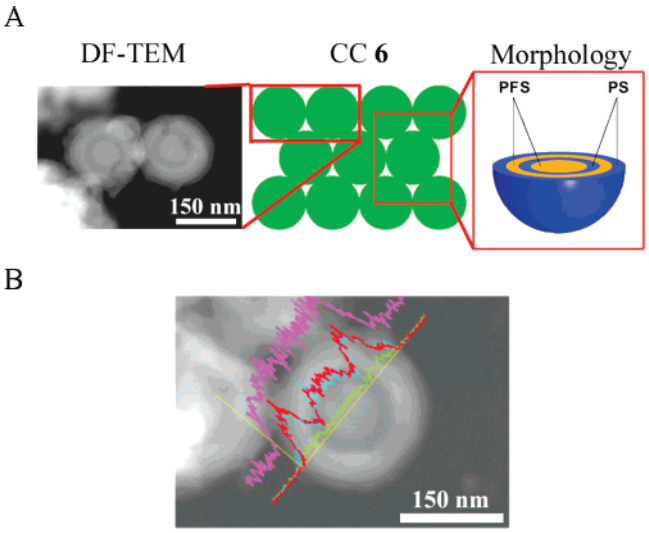

Figure 5. DF-TEM images and depictions of 3-D confined lamella-forming **PS-*b*-PFS (0.52)** in (A) CC $\mathbf{4}_{air}$ (sphere diameter = 210 nm). (B) TEM-EDX line trace (yellow straight line bisecting sphere) of **PS-*b*-PFS (0.52)** in CC $\mathbf{4}_{air}$ (sphere diameter = 210 nm) with C (purple), Fe (red), Si (cyan), and O (green) traces superimposed on the image.

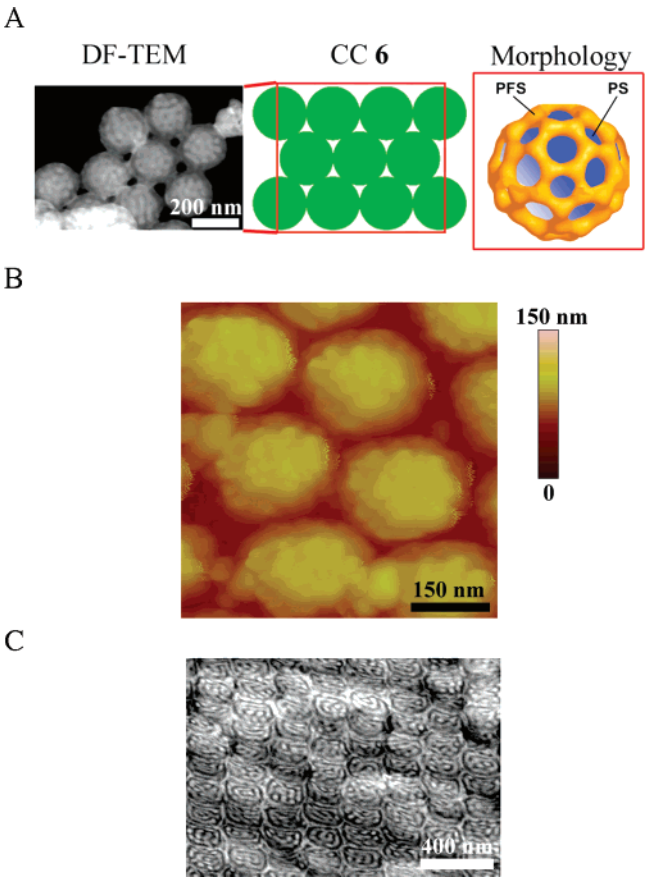

Figure 6. (A) DF-TEM images and depictions of 3-D confined cylinder-forming **PS-*b*-PFS (0.36)** in CC $\mathbf{4}_{air}$ (sphere diameter = 220 nm). (B) SFM of surface of cylinder-forming **PS-*b*-PFS (0.36)** in CC $\mathbf{4}_{air}$. (C) DF-TEM images of sectioned cylinder-forming **PS-*b*-PFS (0.36)** in CC $\mathbf{4}_{air}$.

CC **8**. By priming the scaffold walls of the CC with a **PS** brush layer, preferential surface wetting with matrix-generating **PS** segments from the cylinder-forming **PS-*b*-PFS (0.36)** was expected. The effect of surface wetting of the surface is expected to propagate to the interior of the spherical volume in an alternating fashion and it is anticipated to affect the symmetry

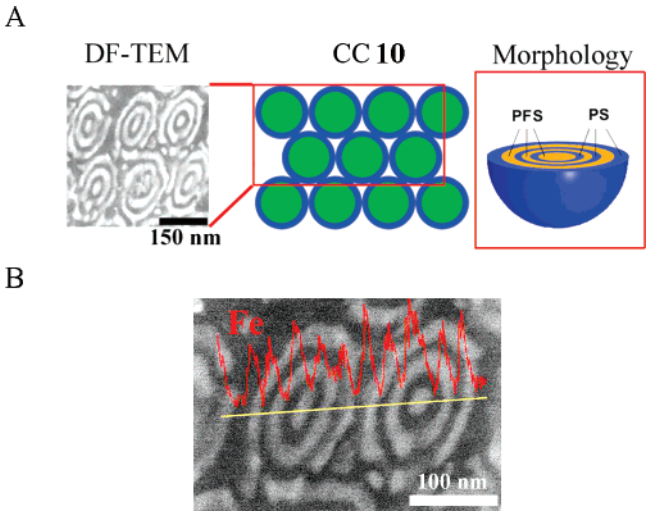

Figure 7. DF-TEM images and depictions of 3-D confined cylinder-forming **PS-*b*-PFS (0.36)** in (A) CC $\mathbf{8}_{PS\ brush/air}$ (sphere diameter = 220 nm). (B) TEM-EDX line trace (yellow straight line bisecting spheres) of **PS-*b*-PFS (0.36)** in CC $\mathbf{8}_{PS\ brush/air}$ (sphere diameter = 220 nm) with Fe (red) trace superimposed on image.

of the diblock copolymer. Shown in Figure 7A is a DF-TEM image of the 3-D confined cylinder-forming **PS-*b*-PFS**. The regular shape of the colloids further confirms the uniformity of the **PS** grafting in CC **8**. The resulting directed morphology is symmetric about a core **PFS** domain (Figure 7). Through use of the Fe-trace EDX spectroscopic line trace that bisects 2 colloids of 3-D confined cylinder-forming **PS-*b*-PFS** (Figure 7B), we confirmed the core-multishell morphology. The generation of the same morphology found for 3-D confined lamellar-forming **PS-*b*-PFS** therefore supports a morphology transition given the use of cylinder-forming **PS-*b*-PFS** in this case.

Controlled Wetting of Templates via a PFS Brush Layer and Resulting Morphology of a 3-D Confined Cylinder-Forming PS-*b*-PFS Block Copolymers as CC 14. An alternative strategy is the confinement of cylinder-forming **PS-*b*-PFS** in a **PFS** brushed CC where the opposite block segments are forced to wet the template. For this situation, we 3-D confined **PS-*b*-PFS (0.36)** using CC $\mathbf{12}_{PFS\ brush/air}$. In this case, by priming the scaffold walls of the CC with a **PFS** brush layer, preferential surface wetting with the cylinder-generating **PFS** segments from the cylinder-forming **PS-*b*-PFS (0.36)** was expected. The effect of wetting of the surface was expected to drastically affect the symmetry and morphology of a 3-D confined diblock copolymer since the minor component **PFS** segments would be forced to interact with the CC template. We have investigated the CC **14** sample with bright-field TEM in order to more effectively visualize the **PFS** brush layer as a dark outer ring. Also, to permit a conceptual 3-D reconstruction of the 3-D morphology, we carefully sectioned this sample using a diamond knife accurately at 75 nm which roughly corresponds to a third of the total sphere diameter. By this technique, a spectrum of images of hexagonally packed disk-like extracts from CC **14** is expected. The location of the **PFS** ring labels the outermost region (see below) and thus permits the 3-D reconstruction of the sample. Shown in Figure 8A are color maps of two arbitrary and touching colloids that represent the close-packed structure in CC **14**. When sections are acquired parallel to and centered at the "equator" of these colloids (shown as a yellow region in Figure 8A), it is anticipated that the circular discs extracted from CC **14** would be in contact with each other. For our purposes, these sections will be referred to an "equatorial belt." If the complementary regions are acquired, henceforth denoted as

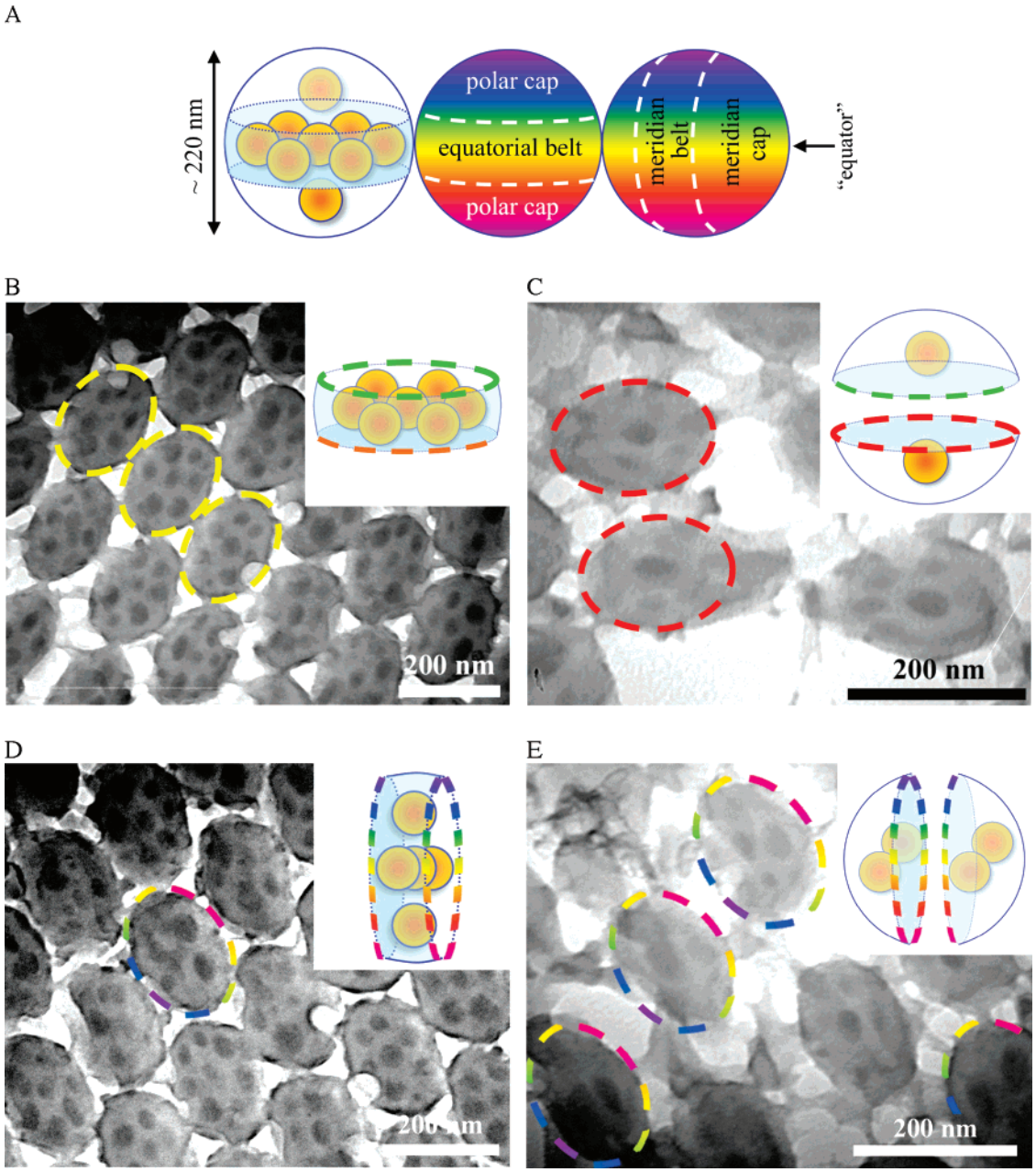

Figure 8. (A) Color map representing regions in CC **14** containing **PS-*b*-PFS (0.36)**. Colored dashed lines in subsequent depictions refer to this color map. Bright Field TEM images and depictions of the outlined morphology (insets) containing (B) the equatorial belt region, (C) the polar cap region, (D) the meridian belt region and (E) the meridian cap region of a colloid from CC **14** with **PS-*b*-PFS (0.36)**.

"polar caps," then separated and lower diameter sections are expected. Furthermore, if by chance extracts of the CC **14** are acquired with an orthogonal orientation with respect to the color maps in Figure 8A, the corresponding sections become "meridian belt" and "meridian caps," respectively.

Shown in Figure 8B−E are BF-TEM images where **PS** domains are now seen as bright phases whereas the **PFS** regions are dark. As inferred by UV−vis characterization, a dark ring should be present at the outermost region of the colloids which would correspond to a **PFS** region consisting of the **PFS** brush layer (∼5 nm) and a wetting contribution from the **PFS** segments from the diblock copolymer. By BF-TEM, a dark **PFS** ring with an estimated thickness of ∼10 nm was found and thus confirms the wetting interaction from the 3-D confined diblock copolymer. Aside from this deliberately engineered **PFS** ring, no "cylinder-like" or "shell-like" **PFS** phases were found for this sample suggesting a morphology transition from those discussed thus far. Additionally, there is little evidence of long-range order and hence limited translation of morphology from one block copolymer colloid to its colloidal neighbors.[48] In many instances, however, hexagonally packed **PFS** domains with the diameters of ∼35−40 nm were observed (see outlined sections in Figure 8B). By arbitrarily assigning this type of disk section as the "equatorial belts" of CC **14**, we are able to begin a conceptual 3-D reconstruction of the confined morphology. Sectional caps of CC **14** with significantly lower diameters are shown in Figure 8C. Centered within each cap is a single well-resolved **PFS** domain with dimensions comparable to those found in the "equatorial belts." On closer inspection, immediately surrounding and centered about this distinct domain are small, faint and out-of-focus **PFS** domains with a hexagonal type arrangement. These faint features represent the portions of the hexagonally packed spheres located in the equatorial belt. It therefore seems likely that the sections observed in Figure 8C are the "polar caps." On the basis of Figure 8, B and C, two conclusions can be drawn thus far. First, the hexagonally

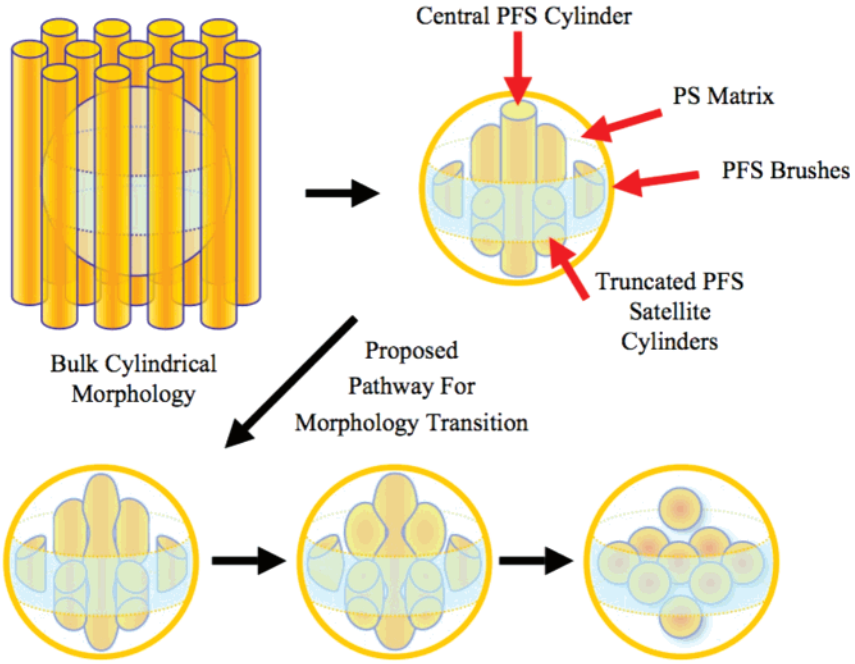

Figure 9. Proposed evolutionary pathway of the transition of a hexagonally packed cylindrical morphology into a spherical morphology in Figure 8A induced by 3-D confinement in CC $\mathbf{12}_{\mathbf{PFS\ brush/air}}$.

packed **PFS** domains in the "equatorial belt" are spherelike in shape, since their dimensions are smaller in the "polar cap". Second, the polar caps contain an additional central **PFS** domain.

Given the preliminary conclusions made from the aforementioned sections of CC **14**, a proposed morphology of the 3-D confined **PS-*b*-PFS (0.36)** in CC $\mathbf{12}_{\mathbf{PFS\ brush/air}}$ is shown in Figure 8A. To confirm this morphology, further investigations by BF-TEM were conducted. Should arbitrary sectioning of the morphology in Figure 8A occur to generate "meridian belt and cap" sections, additional nonhexagonal type arrangements of the **PFS** domains should be present. Shown in the outlined section in the BF-TEM image in Figure 8D is a "meridian belt" section in contact with its colloidal neighbors. Here, a cross-like packing of the **PFS** domains was found and, therefore, confirms that all the **PFS** domains are spherical. Further analysis evidenced "meridian caps" where two **PFS** domains are present along the diameter of the sections (see outlined sections in Figure 8E). These two **PFS** regions represent the bisected **PFS** spheres associated with the "equatorial belt" described above. With these additional images we are therefore able to further justify the proposed morphology of the 3-D confined **PS-*b*-PFS (0.36)** in the **PFS**-brushed CC template.

Interestingly, the important columnar packing of spherical domains in the "meridian belt" lends itself to a proposed mechanism for its origin. Conceptually, the process is depicted in Figure 9, where a bulk hexagonally packed cylindrical morphology is first trapped into a spherical colloid with dimensions similar to those of our system. Clearly the anisotropic character of the cylinder-forming diblock copolymer is in direct conflict with the colloidal surface, which in our case has been predetermined for preferential wetting by **PFS** segments from the block copolymer. The satellite cylindrical domains have been truncated into low aspect ratio domains whereas the central cylindrical domain is more spatially permitted. It is known that under strong external stimuli, such as thermal stress or electronic fields, morphology transitions can occur.[49−53] The cylinder-sphere morphology transition has been modeled theoretically and is known to proceed byway of a wave-like fluctuations associated with the cylindrical domains.[54] The characteristic dimension of the wavelength of the fluctuations is typically similar to that of the cylindrical diameter. With increasing amplitude for these fluctuations, complete dissociation of spherical domains from the cylindrical parent structure occurs. Therefore, in the 3-D confinement of cylinder-forming diblock copolymers with controlled wetting of the template by the minor component block segments, the spatial stress imposed on the block copolymer domains is strong and could follow similar transitional pathways. The resulting cylinder-to-sphere morphology transition to generate the structure in Figure 8A is the result of the combination of the strong curvature as well as the restrictions imposed by spatial and wetting requirements.

Conclusions

The 3-D confinement of lamellar- and cylinder-forming diblock copolymers in silica colloidal and inverse colloidal crystals has been systematically investigated. The morphological effects of 3-D confinement have been accurately documented by way of the excellent electron density contrast and elemental mapping enabled by the polyferrocenylsilane block. A tabular summary of the 3-D confinement of the diblock copolymers investigated herein is shown below (Table 3). Lamella-forming **PS-*b*-PFS** has been used to investigate the effects of inversion with respect to the colloidal crystal template. When the lamellar-forming diblock copolymer occupies tetrahedral and octahedral sites in a silica colloidal crystal, the lamellar domains orient themselves orthogonal to the sphere surfaces. Because of the strong confinement imposed by the surrounding silica spheres the lamellar domains are forced to curve, branch, and join, thus forming a phase that follows the topology of the void space. The ultimate effect is the generation of a tetrapodal and octapodal **PS** domains at the tetrahedral and octahedral sites, respectively. In spite of dramatic changes in the sizes of the silica spheres, defining confinement ratios of $0.89 < D_3/L_0 < 4.1$, this tetrapodal and octapodal morphology persists. For 3-D confinement of lamellar-forming diblock copolymers in inverse silica colloidal crystal with a confinement ratio comparable to that above ($D_3/L_0 = 2.4$), lamellar shells are permitted to orient

Table 3. Summary of 3-D Confinement Results of Lamellar- and Cylinder-Forming Block Copolymers in Colloidal Crystal Templates from Scheme 1

polymer	bulk morphology	brushed surface	colloidal crystal template (D_3)	L_0 (nm)	D_3/L_0	3D confined morphology
PS-*b*-PFS (0.52)	lamellar	none	CC **1** (158 nm/79 nm)[c]	88.0[a]	1.8/0.9[c]	octapods and tetrapods
PS-*b*-PFS (0.52)	lamellar	none	CC **1** (357 nm/179 nm)[c]	88.0[a]	4.1/2.0[c]	octapods and tetrapods
PS-*b*-PFS (0.52)	lamellar	none	CC **4** (210 nm)	88.0[a]	2.4[c]	core-multishell
PS-*b*-PFS (0.36)	hex. PFS cylinders	none	CC **4** (220 nm)	42.5[b]	5.2	golf ball
PS-*b*-PFS (0.36)	hex. PFS cylinders	PS	CC **8** (206 nm)[d]	42.5[b]	4.9[d]	core-multishell
PS-*b*-PFS (0.36)	hex. PFS cylinders	PFS	CC **12** (210 nm)[d]	42.5[b]	4.9[d]	belt hex. packed spheres with 2 spheres, above and below

[a] Estimated from high-resolution TEM images. [b] Bulk $L_0 = 4\pi/(\sqrt{3} \times q^*)$; where q^* is the primary scattering peak as determined by small-angle X-ray scattering. [c] On the basis of $r_{oct} = 0.42R$ and $r_{tet} = 0.21R$ for close packed CC where R is the CC sphere radius. [d] On the basis of volume available after polymer brush applied.

parallel to the templating silica surface thus ultimately generating a spherical **PFS** central core. The resulting core-multishell morphology stresses the importance of curvature in 3-D confined silica colloidal crystal templates.

The more complex 3-D confinement of cylinder-forming diblock copolymers was thoroughly investigated with respect to the wetting properties toward its spherically shaping environment. Without controlled wetting of the silica template, a golf-ball type morphology was found where the interior distribution and morphology are disordered. The generation and use of a **PS**-brushed silica colloidal crystal template was expected to preferentially interact with the matrix-forming **PS** segments of the block copolymer and thus effectively propagate this wetting effect into the interior of the spherical volume in an alternating fashion. Indeed, it was found that this wetting interaction induces an ordering effect based on the generation of a core-multishell morphology, which also represents a cylinder-lamella morphological transition. When the wetting preference was inverted, through use of a **PFS**-brushed silica colloidal crystal template, an ordering effect was also observed. In this case, however, due to the direction of the cylinder-forming **PFS** segments from the diblock copolymer to the surface of the colloid, an interesting morphology transition was detected. Presumably, by forcing the minor component **PFS** to interact with the highly curved spherical surface, significant stress is imposed on the cylinder-forming segments thus leading to a transition to spherical morphology. Through 3-D reconstruction of sectioned samples, the packing of the spherical domains was determined and consists of hexagonally packed spheres in a central belt which separates two additional spheres above and below a central PFS domain.

Our future work includes a theoretical study using Monte Carlo simulation of 3-D confined diblock copolymer morphologies. Additionally, a systematic variation of the dimensions of the colloidal crystal scaffolds will be investigated, and by including sphere-forming **PS-*b*-PFS** in our experiments, the generation of a complete morphology map for 3-D confined diblock copolymers is anticipated. The current results have demonstrated interesting 3-D morphological manipulations governed through tailored interactions with the templates. In terms of physical properties and applications, these materials provide for the first time 3-D periodicity simultaneously at two length scales (one at the scale of light and the other at the scale of nanometers). The periodic arrays should therefore diffract both at the length scale of light and also at the scale of soft X-rays. This would have applications in photonics (e.g., as materials with two photonic bandgaps) and relevant studies are within the scope of our future research.

Experimental Section

Synthesis of PS-*b*-PFS Diblock Copolymers and PFS−OH. The complete synthetic details concerning the synthesis of the **PS-*b*-PFS** materials used in this study have been published elsewhere.[42] The casting of **PS-*b*-PFS** materials was repeated as previously described.[42] Hydroxy-terminated polystyrene (**PS—OH**) was used as received from Polymer Source (M_n = 9900; PDI = 1.04). Hydroxy-terminated polyferrocenyldimethylsilane (**PFS—OH**; M_n = 8100; PDI = 1.17) was synthesized according to literature procedures.[55]

Bulk Casting and Annealing of PS-*b*-PFS. The casting and annealing of the **PS-*b*-PFS** block copolymers into bulk samples was conducted analogously. The representative procedure for **PS-*b*-PFS (0.52)** is described. A concentrated solution of **PS-*b*-PFS (0.52)** (ca. 200 mg/mL) in toluene was applied dropwise to a clean glass slide and was slowly allowed to dry in a closed vial over ca. 5 days. The resulting bulk sample (ca. 1 mm in thickness) was then dried overnight in a vacuum oven at ca. 50 °C. Thermal annealing at ca. 170 °C for 36 h gave the bulk polymer sample as a brittle clear orange material. Small-angle X-ray scattering (SAXS) measurements on films prior to annealing and at 190 °C confirmed that the solvent casting did not result in a nonequilibrium morphology and that at the annealing temperature polymers were in the ordered state. Swelling of the bulk microstructure is thought to be negligible, as neither **PS** nor **PFS** homopolymers were readily soluble in the glue. Room-temperature microtoming was effective, since the glassy **PS** phase provided sufficient integrity for these materials during the sectioning process. Preserved samples were microtomed at a thickness of ca. 100 nm, floated onto water and subsequently transferred to a carbon-coated TEM grid by touching the grid with the floating sections.

Preparation of Silica and Polystyrene Colloidal Crystal Templates (CC $\mathbf{1}_{silica}$ and CC $\mathbf{1}_{PS}$**).** Monodisperse silica spheres were prepared by the controlled hydrolysis of tetraethylorthosilicate according to the Stöber method[56] while a surfactant-free polymerization procedure was used to synthesize monodisperse PS spheres.[57] The sphere solutions were diluted to 0.4 vol % in ethanol, and clean glass slides were then placed vertically into the solution to allow the self-assembly of spheres via solvent evaporation either at an ambient temperature of 35 °C over a period of 3−4 days for small spheres,[58] or at low pressures for large spheres.[59] The colloidal crystal film is essentially single-crystalline with a thickness of ∼20 layers.

Preparation of Silica Inverse Colloidal Crystal Templates (CC $\mathbf{4}_{air}$). Polystyrene colloidal crystal template (CC $\mathbf{1}_{PS}$) was infiltrated with SiO_2 by chemical vapor deposition of alternating $SiCl_4$ and water vapor. The overlayer of SiO_2 was removed by reactive ion etching and then the **PS**−SiO_2 composite was exposed to O_2 plasma in order to remove the polystyrene colloids.

Capillary Infiltration of a CC with PS-*b*-PFS. The representative infiltration of CC $\mathbf{4}_{air}$ with **PS-*b*-PFS (0.36)** is described. A 20 wt % dichloromethane solution of the polymer was allowed to evaporate overnight in the presence of the CC. To ensure complete infiltration samples were annealed using toluene. To eliminate kinetically trapped morphologies using this technique, samples were thermally annealed for 5 days at 170 °C to give the equilibrium structures described in this study.

Grafting PS—OH to CC $\mathbf{4}_{air}$. CC $\mathbf{4}_{air}$ was filled with **PS—OH** according to the procedure outlined for **PS-*b*-PFS** (see above). Grafting of the hydroxy terminus to the silica surface of the CC

was done by a heating under dynamic vacuum (10^{-3} mmHg) at 170 °C for 3 days. Excess **PS—OH** was removed from CC **7** by suspending the sample in a rapidly stirred vial of fresh toluene. The extraction of **PS—OH** was repeated until a constant UV−vis spectrum for CC **8** was found (typically four 4 h extractions). The scalar-wave approximation suggests 17 vol % of the original air sphere is replaced by PS, which translates to a PS layer with a thickness of 7 nm. As a control, CC $\mathbf{4_{air}}$ was heated under dynamic vacuum (10^{-3} mmHg) at 170 °C for 3 days. As a secondary control, CC $\mathbf{4_{air}}$ was filled with **PS—OH** (as above) to produce CC **7**. Without heating under dynamic vacuum for 3 days, it was found that CC **7** could regenerate CC $\mathbf{4_{air}}$ following our toluene extraction procedure (as indicated by UV−vis, see Figure 3A).

Removal of Silica Template in CCs. The silica templates were etched by submerging samples into dilute aqueous HF (~ 5 vol %, ***Caution!***) for 3 h.

Scanning Force Microscopy. Prior to TEM investigations, CC **6** and CC **10** were investigated using SFM. It was found that a semi-ordered dotted surface was only present in CC **6** suggesting that both polymer phases (**PS** and **PFS**) are present at the surface of this sample (see Figure 6B).

Sample Preparation for Transmission Electron Microscopy and Energy Dispersive X-ray Elemental Mapping. Thin sections (~150 nm in thickness) of CC **6** and CC **10** were obtained at room temperature using a Leica Ultracut UCT equipped with a glass knife and collected on carbon coated copper grids (400 mesh). It was found that the bright phases in all DF-TEM were rich in iron and silicon and we confirmed the complete removal of silica with the oxygen trace. In the case of CC **14**, more accurate sectioning was done with a diamond knife at a section thickness of ~75 nm.

Acknowledgment. D.A.R., J.I.L.C., and A.C.A. are grateful to the NSERC and the Government of Ontario for scholarships. G.A.O. is a Government of Canada Research Chair in Materials Chemistry and extends gratitude to the NSERC for sustained support for his work. I.M. acknowledges a Marie-Curie Chair from the European Union and a Royal Society Wolfson Research Merit Award. T.P.R. is thankful for the support of the US DOE Office of Basic Energy Sciences.

References and Notes

(1) Park, C.; Yoon, J.; Thomas, E. L. *Polymer* **2003**, *44*, 6725.
(2) Cheng, J. Y.; Ross, C. A.; Smith, H. I.; Thomas, E. L. *Adv. Mater.* **2006**, *18*, 2505.
(3) Wu, Y.; Cheng, G.; Katsov, K.; Sides, S. W.; Wang, J.; Tang, J.; Fredrickson, G. H.; Moskovits, M.; Stucky, G. D. *Nat. Mater.* **2004**, *3*, 816.
(4) Shin, K.; Xiang, H.; Moon, S. I.; Kim, T.; McCarthy, T. J.; Russell, T. P. *Science* **2004**, *306*, 76.
(5) He, X. H.; Song, M.; Liang, H. J.; Pan, C. Y. *J. Chem. Phys.* **2001**, *114*, 10510.
(6) Sevink, G. J. A.; Zvelindovsky, A. V.; Fraaije, J. G. E. M.; Huinink, H. P. *J. Chem. Phys.* **2001**, *115*, 8226.
(7) Xiang, H.; Shin, K.; Kim, T.; Moon, S. I.; McCarthy, T. J.; Russell, T. P. *Macromolecules* **2004**, *37*, 5660.
(8) Xiang, H.; Shin, K.; Kim, T.; Moon, S. I.; McCarthy, T. J.; Russell, T. P. *Macromolecules* **2005**, *38*, 1055.
(9) Sun, Y. M.; Steinhart, M.; Zschech, D.; Adhikari, R.; Michler, G. H.; Gösele, U. *Macromol. Rapid Commun.* **2005**, *26*, 369.
(10) Liu, Q. Y.; Gao, F.; Komarneni, S.; Mallouk, T. E. *J. Am. Chem. Soc.* **2004**, *126*, 8650.
(11) Thomas, E. L.; Reffner, J. R.; Bellare, J. *J. Phys. (Paris)* **1990**, *52*, C7.363, Suppl. C7.
(12) Wu, Y. Y.; Livneh, T.; Zhang, Y. X.; Cheng, G. S.; Wang, J.; Tang, J.; Moskovits, M.; Stucky, G. D. *Nano Lett.* **2004**, *4*, 2337.
(13) Knoll, A.; Horvat, A.; Lyakhova, K. S.; Krausch, G.; Sevink, G. J. A.; Zvelindovsky, A. V.; Magerle, R. *Phys. Rev. Lett.* **2002**, *89*, 035501.
(14) Coulon, G.; Russell, T. P.; Deline, V. R.; Green, P. F. *Macromolecules* **1989**, *22*, 2581.
(15) Karim, A.; Singh, N.; Sikka, M.; Bates, F. S.; Dozier, W. D.; Felcher, G. P. *J. Chem. Phys.* **1994**, *100*, 1620.
(16) Mansky, P.; Liu, Y.; Huang, E.; Russell, T. P.; Hawker, C. J. *Science* **1997**, *275*, 1458.
(17) Rockford, L.; Liu, Y.; Mansky, P.; Russell, T. P.; Hawker, C. J. *Phys. Rev. Lett.* **1999**, *82*, 2602.
(18) Edwards, E. W.; Montague, M. F.; Solak, H. H.; Hawker, C. J.; Nealey, P. F. *Adv. Mater.* **2004**, *16*, 1315.
(19) Bates, F. S.; Fredrickson, G. H. *Annu. Rev. Phys. Chem.* **1990**, *41*, 525.
(20) Turner, M. S. *Phys. Rev. Lett.* **1992**, *69*, 1788.
(21) Shull, K. R. *Macromolecules* **1992**, *25*, 2122.
(22) Kikuchi, M.; Binder, K. *Europhys. Lett.* **1993**, *21*, 427.
(23) Walton, D. G.; Kellogg, G. J.; Mayes, A. M.; Lambooy, P.; Russell, T. P. *Macromolecules* **1994**, *27*, 6225.
(24) Lambooy, P.; Russell, T. P.; Kellogg, G. J.; Mayes, A. M.; Gallagher, P. D.; Satija, S. K. *Phys. Rev. Lett.* **1994**, *72*, 2899.
(25) Brown, G.; Chakrabarti, A. *J. Chem. Phys.* **1995**, *102*, 1440.
(26) Koneripalli, N.; Singh, N.; Levicky, R.; Bates, F. S.; Gallagher, P. D.; Satija, S. K. *Macromolecules* **1995**, *28*, 2897.
(27) Kellogg, G. J.; Walton, D. G.; Mayes, A. M.; Lambooy, P.; Russell, T. P.; Gallagher, P. D.; Satija, S. K. *Phys. Rev. Lett.* **1996**, *76*, 2503.
(28) Matsen, M. W. *J. Chem. Phys.* **1997**, *106*, 7781.
(29) Pickett, G.; Balazs, A. C. *Macromol. Theory Simul.* **1998**, *7*, 249.
(30) Fasolka, M. J.; Banerjee, P.; Mayes, A. M.; Pickett, G.; Balazs, A. C. *Macromolecules* **2000**, *33*, 5702.
(31) Tang, W. H. *Macromolecules* **2000**, *33*, 1370.
(32) Arsenault, A. C.; Rider, D. A.; Tétreault, N.; Chen, J. I. L.; Coombs, N.; Ozin, G. A.; Manners, I. *J. Am. Chem. Soc.* **2005**, *127*, 9954.
(33) Kulbaba, K.; Manners, I. *Macromol. Rapid Commun.* **2001**, *22*, 711.
(34) MacLachlan, M. J.; Ginzburg, M.; Coombs, N.; Coyle, T. W.; Raju, N. P.; Greedan, J. E.; Ozin, G. A.; Manners, I. *Science* **2000**, *287*, 1460.
(35) Ginzburg, M.; MacLachlan, M. J.; Yang, S. M.; Coombs, N.; Coyle, T. W.; Raju, N. P.; Greedan, J. E.; Herber, R. H.; Ozin, G. A.; Manners, I. *J. Am. Chem. Soc.* **2002**, *124*, 2625.
(36) Lastella, S.; Jung, Y. J.; Yang, H.; Vajtai, R.; Ajayan, P. M.; Ryu, C. Y.; Rider, D. A.; Manners, I. *J. Mater. Chem.* **2004**, *14*, 1791.
(37) Hinderling, C.; Keles, Y.; Stoeckli, T.; Knapp, H. F.; De Los Arcos, T.; Oelhafen, P.; Korczagin, I.; Hempenius, M. A.; Vancso, G. J.; Pugin, R.; Heinzelmann, H. *Adv. Mater.* **2004**, *16*, 876.
(38) Whittell, G. R.; Manners, I. *Adv. Mater.* **2007**, *19*, 3439.
(39) Eitouni, H. B.; Balsara, N. P. *J. Am. Chem. Soc.* **2006**, *128*, 16248.
(40) Ma, Y.; Dong, W.-F.; Hempenius, M. A.; Möhwald, H.; Vancso, G. J. *Nat. Mater.* **2006**, *5*, 724.
(41) Arsenault, A. C.; Puzzo, D. P.; Manners, I.; Ozin, G. A. *Nature Photonics* **2007**, *1*, 468.
(42) Rider, D. A.; Cavicchi, K. A.; Power-Billard, K. N.; Russell, T. P.; Manners, I. *Macromolecules* **2005**, *38*, 6931.
(43) Lu, J. Q.; Kopley, T. E.; Moll, N.; Roitman, D.; Chamberlin, D.; Fu, Q.; Liu, J.; Russell, T. P.; Rider, D. A.; Winnik, M. A.; Manners, I. *Chem. Mater.* **2005**, *17*, 2227.
(44) Mittleman, D.; Bertone, J. F.; Jian, P.; Hwang, K. V.; Colvin, V. L. *J. Chem. Phys.* **1999**, *111*, 345.
(45) Arsenault, A. C.; Halfyard, J.; Wang, Z.; Kitaev, V.; Ozin, G. A.; Manners, I.; Mihi, A.; Miguez, H. *Langmuir* **2005**, *21*, 499.
(46) For the analogous 2-dimensionally confined lamella-forming polystyrene-block-polybutadiene diblock copolymers, "onion-like" morphologies with changing dimensions for the lamellar periodicity as a function of the distance from the core have also been observed. Please see ref 7.
(47) Polymer nano- and microspheres with bumpy and chain-segregated surfaces with a similar structure have recently been observed. Please see: Zheng, R.; Liu, G.; Yan, X. *J. Am. Chem. Soc.* **2005**, *127*, 15358.
(48) To date, we have only observed PS-*b*-PFS domains uniformly traversing from neighboring colloids when larger CC **4** air scaffolds are used (~350 nm diameter). It is possible that with the smaller CC $\mathbf{12_{PFS\ brush/air}}$ scaffolds used herein that morphological translation from one block copolymer region to its neighbors is spatially inhibited allowing most block copolymer colloids to exhibit semi-independent morphology and orientation.
(49) Ryu, C. Y.; Vigild, M. E.; Lodge, T. P. *Phys. Rev. Lett.* **1998**, *81*, 5354.
(50) Ryu, C. Y.; Lodge, T. P. *Macromolecules* **1999**, *32*, 7190.
(51) Kimishima, K.; Koga, T.; Hashimoto, T. *Macromolecules* **2000**, *33*, 968.
(52) Sakurai, S.; Hashimoto, T.; Fetters, L. J. *Macromolecules* **1996**, *29*, 740.
(53) Sota, N.; Sakamoto, N.; Saijo, K.; Hashimoto, T. *Macromolecules* **2003**, *36*, 4534.
(54) Xu, T.; Zvelindovsky, A. V.; Sevink, G. J. A.; Lyakhova, K. S.; Jinnai, H.; Russell, T. P. *Macromolecules* **2005**, *38*, 10788.

(55) Korczagin, I.; Hempenius, M. A.; Vancso, G. J. *Macromolecules* **2004**, *37*, 1686.
(56) Stöber, W.; Fink, A.; Bohn, E. J. *J. Colloid Interface Sci.* **1968**, *26*, 62.
(57) Shouldice, G. T. D.; Vandezande, G. A.; Rudin, A. *Eur. Polym. J.* **1994**, *30*, 179.
(58) Jiang, P.; Bertone, J. F.; Hwang, K. S.; Colvin, V. L. *Chem. Mater.* **1999**, *11*, 2132.
(59) Vekris, E.; Kitaev, V.; von Freymann, G.; Perovic, D. D.; Aitchison, J. S.; Ozin, G. A. *Adv. Mater.* **2005**, *17*, 1269.

MA7020248